Live fast and die young

Evolution and fate of massive stars

Renzo, M.

Publication date
2019

Document Version
Other version

License
Other

Chapter 6

Mind the gap: The location of the pair instability supernovae black hole mass gap

R. Farmer, M. Renzo, S. E. de Mink, P. Marchant, S. Justham

Submitted to ApJ

Abstract

In the era of gravitational wave astronomy, detailed knowledge of the birth mass function of black holes (BHs) is necessary to interpret and understand already observed and upcoming gravitational-wave detections. At the upper edge of the BH mass distribution, pair instability supernovae (PISN) predict the existence of a gap in the BH mass distribution, while their lower mass counterparts, pulsational-pair-instability supernovae, set the maximum BH mass below such gap. Using the MESA stellar evolution code we investigate the location of this mass gap and its sensitivity to both the metallicity of the progenitors and uncertain physics including nuclear reaction rates, chemical mixing, neutrino physics, and wind mass loss. We find that the location of the mass gap is not sensitive to the metallicity, and hence not to the host galaxy of the stellar progenitors. Therefore, if the population of BHs revealed by gravitational-wave detections is dominated by stellar BHs, the location of the gap can be used as a "standard siren" across the Universe. However, the maximum BH mass below the gap is sensitive to the $^{12}C(\alpha,\gamma)^{16}O$ reaction rate: as the rate decreases the maximum BH mass increases. A $\pm1\sigma$ variation of this rate translates to a $16\,M_{\odot}$ variation in the maximum BH mass, from $40\,M_{\odot}$ to $56\,M_{\odot}$. Thus, we propose that the detection of merging BHs can constrain nuclear astrophysics, by detecting the most massive stellar BH in the Universe.

6.1 Introduction

The detection of merging black hole (BH) binaries through gravitational waves (e.g., LVC 2016c, 2018b) has opened an observational window on the most massive stellar BHs in the Universe. Stellar evolution theory predicts the existence of a gap in the BH mass distribution due to pair-instability evolution (Fowler & Hoyle 1964; Barkat et al. 1967; Woosley 2017), and the current population of detected binary BHs are consistent with a lack of BHs with masses $\geq 45\ M_{\odot}$ (LVC 2016c,a, 2017b,c,d). So far, the most massive BH found is the primary of GW170729, with a mass of $50.6^{+16.6}_{-10.2}\ M_{\odot}$ (LVC 2018a). This object is at the edge of the theoretically predicted mass gap. Fishbach & Holz (2017) showed that the existence of the gap and the maximum BH mass at its lower edge can be significantly constrained with the detections expected during the third LIGO/Virgo observing run.

The existence of this pair-instability BH mass gap is expected because of the occurrence of pair-instability supernovae (PISN) which can completely disrupt the progenitor star leaving no compact remnant behind (Rakavy & Shaviv 1967; Fraley 1968; Woosley et al. 2002). However, it is pulsational pair instability supernovae (PPISN) that set the lower edge of this PISN BH mass gap. PPISN are predicted for stars slightly less massive than PISN progenitors, and they leave behind a BH, but only after having experienced several episodes of pulsational mass loss, which reduce the mass of the final BH.

Here, we investigate the location of the BH mass gap due to PPISN (Rakavy & Shaviv 1967; Fraley 1968), and in particular its lower boundary, i.e., how massive can the most massive BH below the gap be. Single stars with initial masses $100\ M_{\odot} \lesssim M_{\rm ZAMS} \lesssim 140\ M_{\odot}$ (or equivalently final helium core masses of $32\ M_{\odot} \lesssim M_{\rm He} \lesssim 60\ M_{\odot}$), are expected to undergo pulsation pair instabilities (PPI) (Woosley et al. 2002; Chen et al. 2014; Yoshida et al. 2016; Woosley 2017). This instability results in a series of pulses, each removing mass from the star. Eventually, the core stabilizes, the pulses cease, and the star ends its evolution in an iron core collapse (CC) most likely producing a BH (Barkat et al. 1967; Woosley 2017).

More massive stars are fully disrupted instead of producing ever more massive BHs: for initial masses $140\ M_{\odot} \lesssim M_{\rm ZAMS} \lesssim 260\ M_{\odot}$ (metallicity dependant), corresponding roughly to final helium cores $60\ M_{\odot} \lesssim M_{\rm He} \lesssim 140\ M_{\odot}$ (Heger & Woosley 2002), the first pulse is so violent that the entire star is fully disrupted in a PISN (Woosley et al. 2002; Heger et al. 2003), without any BH remnant formed. For even higher initial masses, corresponding to final $M_{\rm He} \gtrsim 130\,M_{\odot}$, the photodisintegration instability allows again for BH formation (Heger et al. 2003), closing the PISN BH mass gap from above.

From a population of binary BH mergers, we can determine their rate (LVC 2016a), and their mass distribution (Cutler & Flanagan 1994; Kovetz et al. 2017). However, the time-scale for binary BHs to merge can be of the order of giga-years (Paczyński 1967). Therefore, even if determining the host galaxy is possible despite the limited spatial localization of binary BH mergers the local observed population of stars may have formed later and hence have a different metallicity to that of the BH progenitor. This complicates estimating the rate of BH formation (Portegies Zwart & McMillan 2000b; Dominik et al. 2012; LVC 2016c), since this estimate requires knowing the star formation rate and metallicity evolution of the Universe (Madau & Dickinson 2014; Neijssel et al. 2019).

The maximum BH mass below the PISN gap however can be more easily determined (LVC 2018b) as it is independent of the rate of BH formation. We can thus use it without knowing the metallicity dependant star formation rate of the Universe. In this study we explore how sensitive the maximum BH mass is to uncertainties in the metallicity of the progenitors as well as other known uncertainties in our understanding of stellar physics.

In Sec. 6.2 we describe the evolution of PPISN and PISN while introducing our computational approach. We outline the parameter variations we consider in Sec. 6.3. In Sec. 6.4 we discuss the sensitivity of the maximum BH mass to changes in the metallicity of the stellar progenitors. Sec. 6.5 explores how uncertain the maximum BH mass below the PISN mass gap is because of uncertainties in the assumed input physics. We discuss the implications of the maximum BH mass in Sec. 6.6. We conclude and summarize our results in Sec. 6.7 and 6.8.

6.2 Evolution through the pulses

Using `MESA` version[1] 11123 (Paxton et al. 2011, 2013, 2015, 2018), we evolve a series of single bare helium cores until they undergo either PPI followed by a core collapse supernovae (PPISN) or the more violent pair instability that fully disrupts the star in a PISN. Input files necessary to reproduce this work and the resulting output files are made freely available at www.mesastar.org[2].

Marchant et al. (2018), we evolve systems around the lower edge of Based on the results of the PISN BH mass gap, with initial helium core masses between $30 - 105\,M_{\odot}$. We chose to evolve bare helium cores as stars in this mass range are expected to lose their hydrogen-rich envelope long before their death. This could happen either through binary interactions (Kobulnicky & Fryer 2007; Sana et al. 2012; Almeida et al. 2017), strong stellar winds (Vink & de Koter 2005; Renzo et al. 2017), LBV-like mass loss (Humphreys & Davidson 1994), or because of chemically homogeneous evolution due to fast rotation Maeder & Meynet (2000); Yoon et al. (2006); de Mink et al. (2009); Mandel & de Mink (2016); Marchant et al. (2016).

As stars evolve from the zero age helium branch (ZAHB) they proceed by burning helium convectively in their core which encompasses $\sim 90\%$ of the mass, taking $\sim 10^5$ years. Once helium has been burnt in the core convection ceases, leaving behind a carbon/oxygen (CO) core with an outer helium burning shell surrounded by a helium-rich surface layer. For sufficiently massive cores an inner region of the star will enter the pair instability region. Due to dynamical instability from the production of $e^{\pm}$ pairs softening the equation of state the core begins contracting and heating up. Eventually this region will heat up sufficiently to ignite the residual carbon and explosively ignite the oxygen (Fowler & Hoyle 1964; Rakavy & Shaviv

[1] This version is not an official release, but it is publicly available from http://mesa.sourceforge.net/

[2] As well as http://doi.org/10.5281/zenodo.3346593

1967; Barkat et al. 1967).

This ignition will reverse the contraction and may generate an outwardly propagating pulse, if the star was sufficiently massive. As this pulse propagates outwards the inner region of the star expands and cools. Once the pulse reaches the surface, it steepens into a shock wave which can then accelerate material beyond the escape velocity. This removes between a few tenths and a few tens of solar masses of material in a pulsational mass loss episode (PPI) (Yoshida et al. 2016; Marchant et al. 2018; Woosley 2019). Some stars will undergo "weak" pulsations, these stars undergo PPI instabilities but do not drive a shock sufficient to remove mass (Woosley 2017; Marchant et al. 2018). To focus on the impact that this process has on the BH masses, in this study we define only systems which can drive mass loss as undergoing a pulse. We define weak pulses as ones only able to drive small amounts of mass loss $\sim 0.1\,M_{\odot}$ per pulse, while strong pulses drive up to several tens of solar masses lost per pulse. The star then contracts and cools either via neutrinos or in the most massive cores undergoing PPIs via radiative loses. This cycle of contraction and ignition can occur multiple times.

This contraction and expansion process is hydrodynamical in nature, generating multiple shocks. To model these shocks we uses `MESA`'s HLLC contact solver (Toro et al. 1994; Paxton et al. 2018) However for computational reasons we do not use the HLLC solver while the star is in hydrostatic equilibrium. Instead, only as the star evolves away from hydrostatic equilibrium do we switch to using the HLLC solver. We then follow the hydrodynamics through the ignition and expansion of the star. Once all secondary shocks have reached the surface, we excise any material that has a velocity greater than the escape velocity (Yoshida et al. 2016; Marchant et al. 2018). We then create a new stellar model with the same mass, chemical composition, and entropy as the previous model had (minus the excised material). At this point we switch back to using `MESA`'s hydrostatic solver as the star can be approximated as being in hydrostatic equilibrium. This model is then evolved until the next pulse, where this process repeats, or on to core collapse, which is defined when any part of the star infalls with $v > 8\,000\,\mathrm{km\,s^{-1}}$. Stars which undergo a PISN are evolved until all stellar material becomes unbound.

We define the time just before a pulse to be when the pressure weighted integral of $\langle\Gamma_1\rangle < 4/3$ (Stothers 1999; Marchant et al. 2018). A special case occurs once the core temperature ($\mathrm{T_c}$) exceeds $\mathrm{T_c} > 10^{9.6}$K, when we continue using the HLLC solver as the star is approaching CC. During the hydrodynamical phases we turn off mass loss from winds. Given the short amount of physical time spent by our models during the hydrodynamical phase of evolution and the typical wind mass loss rates of $\sim 10^{-5}\ M_{\odot}\ \mathrm{yr^{-1}}$, this does not influence significantly the final BH masses.

We define the mass of the BH formed to be the mass enclosed with a binding energy $> 10^{48}\mathrm{erg\ s^{-1}}$ (e.g., Nadezhin 1980; Lovegrove & Woosley 2013) and velocities less than the escape velocity, measured at iron core collapse. Stars which undergo a PISN are expected to be fully disrupted and thus leave no remnant behind. The final BH mass may depend on the mass of neutrinos lost during the collapse, assuming they are not accreted into the

BH (Coughlin et al. 2018). Without a fully consistent theory for BH formation, we use this simple value based on the binding energy, which provides an upper limit on the BH mass. In general this limit is $\sim 0.01\ M_{\odot}$ smaller than the total mass of bound material at core collapse. We define the location in mass of the CO core at the end of core helium burning where $X(^{12}\mathrm{C}) > 0.01$ and $X(^{4}\mathrm{He}) < 0.01$.

6.3 Choice of parameters

There are many uncertain ingredients in the modelling of stars. These can either be algorithmic parameters that are insufficiently constrained by experiments or observations (e.g., convective mixing) or physical quantities that can only be measured in regimes which are much different than the stellar case and require complicated and uncertain extrapolation for their applications to stars (e.g., nuclear reaction rates). Thus we model a range of systems, with differing environmental, physical, and numerical parameters to test the sensitivity of our results to these parameters.

6.3.1 Metallicity

Since LIGO has the ability to detect stellar mass BH mergers out to red-shifts ~ 1, for stellar mass BHs, and the potential for the progenitor stars to come from even earlier epochs it can thus probe the history of star formation across the Universe (LVC 2018b) Thus we evolve a series of models with varying metallicities (Z) between 10^{-5} and 4×10^{-3}. The lower limit results in stars that do not not lose any significant amount of mass though winds. The upper limit is set by the requirement for the most massive BH, below the PISN mass gap, to come from a PPISN instead of direct CC (Langer et al. 2007). At higher metallicities stars lose sufficient mass that they do not enter the pair instability region and instead evolve in hydrostatic equilibrium though carbon, oxygen, and silicon burning and then undergo direct collapse, likely forming a BH when they try to burn iron. Our fiducial metallicity, when varying other physics parameters, is $Z = 10^{-3}$.

6.3.2 Wind mass loss

The total mass a star loses during its evolution plays a critical role in the fate of the star, however just as important is how and when it loses the mass. Mass loss via winds is not self-consistently solved in 1D stellar evolution models, but instead, is set by a mass loss prescription and that functional form can have a large impact on the star's evolution (Renzo et al. 2017).

We investigate three different wind mass loss algorithms, each having a different dependence on the stellar properties: the prescription of Hamann et al. (1982, 1995); Hamann & Koesterke (1998) (H); the prescription of Nugis & Lamers (2000) (N&L); the prescription of Tramper et al. (2016) (T); as well as no mass loss ($\dot{M} = 0$).

The helium cores we investigate have surface luminosities $\sim 10^6\, L_{\odot}$, which is at the upper edge of currently known Wolf-Rayet stars used to derive these prescriptions. Thus we also append a free scaling factor η to test possible uncertainties in our knowledge of mass loss rates in high luminosity helium cores. This free scaling parameter can be related to the inhomogeneities in the wind structure (so-called "clumpiness") with $\eta = \sqrt{\langle\rho^2\rangle/\langle\rho^2\rangle}$, where ρ is the wind mass density, and the angle brackets indicate the spatial average over the stellar surface. We vary η between 0.1 and 1.0 (Smith 2014), with our fiducial wind being the (H) rate with $\eta = 0.1$ (Yoon et al. 2010).

6.3.3 Neutrino physics

The evolution of massive stars is governed by neutrino losses, as the star evolves to higher core temperatures and densities the rate of thermal neutrino losses increases. Stars undergoing pulsational instabilities are also sensitive to the neutrino cooling rates, as due to the generation of $e^{\pm}$ they produce copious amounts of neutrinos from their annihilation which leads to the core cooling. The stronger the cooling, the more energy is required from nuclear burning to overcome these loses.

MESA implements the analytic fits to neutrino losses from Itoh et al. (1996) for pair, photo, plasma, bremsstrahlung and recombination neutrino processes. These fits have a quoted uncertainties of $\sim 10\%$ for pair, $\sim 1\%$ for photo, $\sim 5\%$ for plasma, $\sim 10\%$ for recombination, neutrinos compared to the detailed calculations for the regions where these processes are dominant (Itoh et al. 1996). Outside of the dominant regions the error increases rapidly. Bremsstrahlung neutrino losses have no quoted error, thus we assume a $\sim 10\%$ error, similar to the other processes. We assume these errors to be 1σ values. We vary the neutrino rates between $\pm 3\sigma$ of their quoted rates. While Itoh et al. (1996) states that the analytic fits will generally under predict the true value, we test both over and under estimates for completeness.

A second important factor for the rate of neutrino loss in stars is the Weinberg angle, or the weak mixing angle from the Weinberg-Salam theory of the electroweak interaction (Weinberg 1967; Salam 1968). In the analytical fits of Itoh et al. (1996), the Weinberg angle sets the relative rate of neutrino production between neutral current reactions and charged current neutrino reactions. Increasing the Weinberg angle increases the neutrino cooling rate, by increasing the fraction of charged current reactions. While individual measurements of the Weinberg angle have small quoted uncertainties, there is an systematic offset between different values which is larger than the quoted uncertainties. Thus we model three values for the Weinberg angle 0.2319 (Itoh et al. 1996, our fiducial value), 0.23867 (Erler & Ramsey-Musolf 2005), and 0.2223 (Mohr et al. 2016).

6.3.4 Mixing

Convection inside a star is a difficult process to model (Böhm-Vitense 1958; Canuto et al. 1996; Meakin & Arnett 2007a), especially during dynamical phases of a star's evolution

(Chatzopoulos et al. 2014, 2016). Thus, we take a simpler approach and restrict ourselves to testing uncertainties within the framework of mixing length theory (MLT). Specifically, we test the MLT's α_{mlt} efficiency parameter between 1.5 and 2.0, with 2.0 being our fiducial value. While this may not capture the true uncertainty due to convection, it can provide bounds on the result. We use the prescription of convective velocities from Marchant et al. (2018) to limit the acceleration of convective regions.

At the convective boundaries we assume convective overshoot mixing with an exponential profile. This is parameterized into two terms, f_{ov} and f_0, the first term dictates the scale height of the convective overshoot, in units of the pressure scale height. The second term dictates the starting point inside the convective boundary from where the overshoot begins, in pressure scale heights (Paxton et al. 2011). We assume the value of $f_0 = 0.005$, and vary f_{ov} between 0.0 (no overshooting) and 0.05, with $f_{\mathrm{ov}} = 0.01$ being our fiducial value.

6.3.5 Nuclear physics

Nuclear reaction rates are highly sensitive to the temperature of at which the reaction occurs, and due to this sensitivity the uncertainty in the rate is also highly temperature dependent (Iliadis et al. 2010a,b; Longland et al. 2010). Varying nuclear reaction rate within its known uncertainties has been shown to a have large impact on the stellar structure of a star (Hoffman et al. 1999; Iliadis et al. 2002; Fields et al. 2016, 2018).

We vary several nuclear reaction rates between their $\pm 1\sigma$ uncertainties with data from `STARLIB` (Sallaska et al. 2013). `MESA`'s default rate set is a combination of `NACRE` (Angulo et al. 1999a) and `REACLIB` (Cyburt et al. 2010). To sample the rates, we take the median value from `STARLIB` and by taking the uncertainty on a rate to be a log normal distribution we can compute both an upper and lower rate (given by $\pm 1\sigma$) to cover 68% of the rate's probability distribution. These bounds vary as a function of temperature reflecting the varying uncertainty in the underlying experimental data. When sampling the rates, we vary only one rate at a time, with the reminder of the rates being taken from `NACRE` and `REACLIB`. Correlations between rates can impact the structure of a star and deserve further study (Fields et al. 2016, 2018).

We test variations in three rates; 3α is the triple alpha reaction, C12α is the $^{12}\mathrm{C}(\alpha,\gamma)^{16}\mathrm{O}$ reaction, and O16α is the $^{16}\mathrm{O}\,(\alpha,\gamma)^{20}\,\mathrm{Ne}$ reaction. We choose to vary only a few rates over their 1σ uncertainties to limit the computational cost.

We also investigate the effect of changing the nuclear network used, which can have a large impact on the evolution of massive stars (Farmer et al. 2016). By default we use the `approx21.net` which follows alpha chain reactions from carbon and iron (Timmes 1999; Timmes et al. 2000). We also evolve models with both `mesa_75.net`, which has 75 isotopes up to ^{60}Zn, and `mesa_128.net`, which has 128 isotopes up to ^{60}Zn, including more neutron rich nuclei than the `mesa_75.net` network.

6.3.6 Other physics

MESA is built upon a range of other physics, which we do not vary here but which can provide other uncertainties in the modelling of massive stars. MESA's equation of state (EOS) for massive stars is a blend of the OPAL (Rogers & Nayfonov 2002) and HELM (Timmes & Swesty 2000) EOSes. Radiative opacities are primarily from OPAL (Iglesias & Rogers 1993, 1996b), with low-temperature data from Ferguson et al. (2005) and the high-temperature, Compton-scattering dominated regime by Buchler & Yueh (1976). Electron conduction opacities are from Cassisi et al. (2007). Nuclear screening corrections come from Salpeter (1954); Dewitt et al. (1973); Alastuey & Jancovici (1978); Itoh et al. (1979).

6.4 Robustness of the gap to metallicity

Figure 6.1 shows the predicted mass of the BH formed from a helium star with a mass between between $30-100\,M_{\odot}$ and initial metallicities between $Z=10^{-5}$ and 4×10^{-3}. At first, as the helium core mass increases, so does the resulting BH mass due to the larger initial mass of the star. However, once the star enters the pulsational regime, it begins to lose mass and eventually the amount of mass loss via pulses is sufficient to lower the final BH mass. This turn over occurs due to changes in the behavior of the PPI pulses. As the core mass increases, the pulses decrease in number but become more energetic, driving off more mass in each pulse. At the edge of the PISN region, the helium cores can lose $\sim 10\ M_{\odot}$ of material in a single pulse.

As the core mass is increased further, the first pulse becomes energetic enough for the star to be completely disrupted in a PISN. At the lower edge of the BH gap, the most massive helium stars under going PPI mass loss without being disrupted lose several tens of solar masses of material per pulse, leaving behind BHs of $\sim 15\,M_{\odot}$. The lowest mass a BH may have, after undergoing PPISN, is set by the production of ^{56}Ni inside the star. As the initial mass of the star increases, more ^{56}Ni is produced inside the star. Eventually sufficient ^{56}Ni is produced to unbind any material that was not initially driven away the pulses (Marchant et al. 2018). However the exact edge of the PPISN/PISN boundary, and thus the minimum BH mass produced by PPISN, is not resolved given our grid spacing.

As the initial metallicity of the star increases the mass of the BH decreases, for fixed initial helium core mass. This is due to increases in the amount of mass lost via winds before the star enters the PPI region, which decreases the final mass of the star before collapse. The progressive shift to the right of the hatched region in Figure 6.1 with increasing Z shows that the minimum (and maximum) initial helium core mass needed to undergo pulsations also increases as the metallicity increases. Again this is due to the winds; as the winds become stronger we require an initially more massive progenitor star to retain sufficient mass to undergo pulsations.

Figure 6.2 shows the BH mass as a function of the CO core mass over our metallicity range. Here we see a much tighter relationship between the CO core mass and the final BH

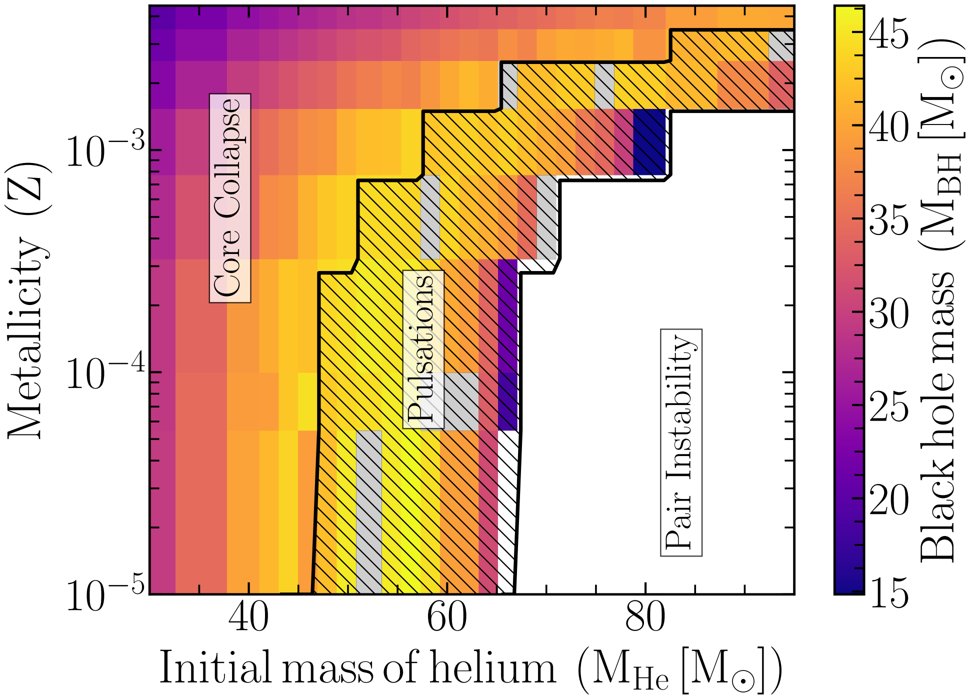

Fig. 6.1: The mass of the BH formed as function of the metallicity of the star and its initial helium star mass. The hashed region denotes those models which undergo pulsational mass loss. Grey regions indicate models which do not reach CC due to numerical issues.

mass than in Figure 6.1 between the initial helium core mass and final BH mass. We find strong PPI pulses removing significant amount of mass between CO core masses $M_{CO} \simeq 38\,M_\odot$ and $M_{CO} \simeq 60\,M_\odot$. The upper edge of the PPISN region slightly decreases to $M_{CO} = 56\,M_\odot$ as the metallicity increases. The most massive BHs come from stars with $M_{CO} \simeq 50\,M_\odot$, not from those with the most massive CO cores that undergo a PPI (in Figure 6.1 these are $M_{CO} \simeq 60\,M_\odot$). This is due the pulses becoming stronger and thus driving more mass loss.

We attribute the differences arising from changes in metallicity primarily due to the differences in wind mass loss rate. Higher metallicity stars have higher wind mass loss rates which can drive larger variations, pre-pulse, in the core structure (Castor et al. 1975; Vink et al. 2001). At the highest metallicities the stellar winds have also removed all remaining helium from the star and have begin ejecting C/O rich material, pre-pulses. Thus these progenitors would likely look like carbon or oxygen rich Wolf-Rayet (WC/WO) stars before pulsating. This justifies our choice of using the CO core mass over the He core mass as a better proxy for the final BH masses. We note that while the CO-BH mass distribution is relativity constant over the metallicities considered here, the BH formation rate, and hence the merger rate, will

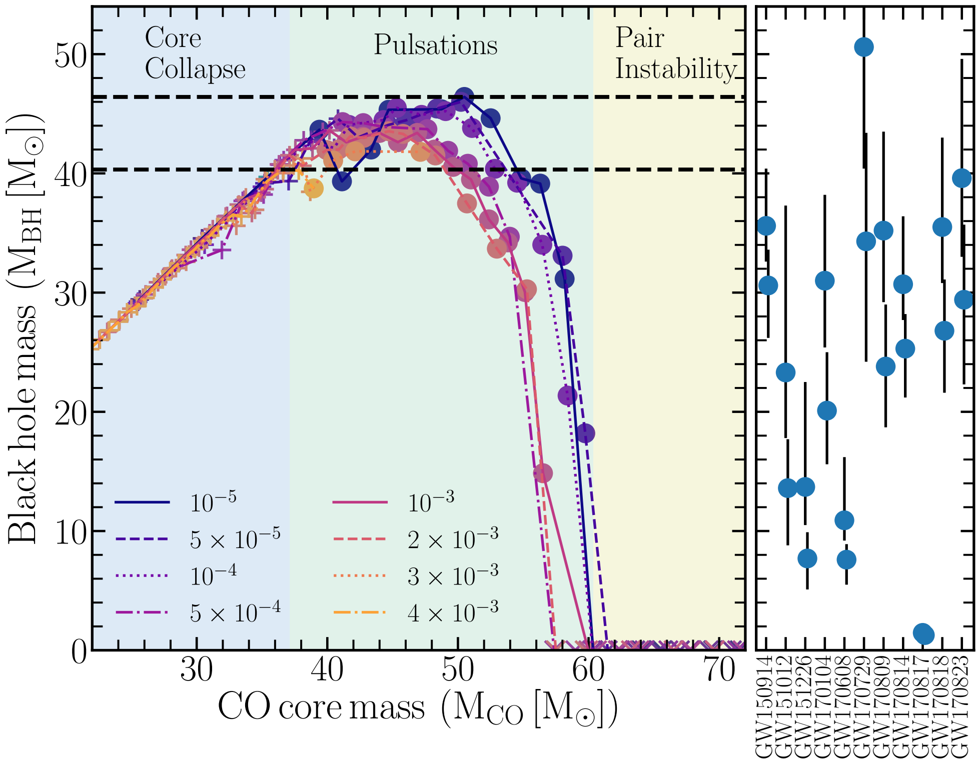

Fig. 6.2: Mass of final BH as a function of the CO core mass, for different metallicities. Circles denote models that underwent at least one pulse, pluses evolved to directly CC, and crosses undergo a PISN. The left blue region denotes where models undergo CC, the middle green region denotes PPISN, while the right yellow region denotes PISN, as determined by stars with $Z = 10^{-5}$. Points in the right panel show the current median mass estimates for the double compact objects detected by LIGO/VIRGO with their 90% confidence intervals (LVC 2018b). Dashed horizontal lines emphasize the maximum spread in the locations for the edge of the BH mass gap, or in other words the spread in the maximum BH mass below the PISN BH mass gap.

vary as a function of metallicity. This is due to changes in the initial stellar mass needed to form such massive CO cores.

The right panel of Figure 6.2 also shows a comparison with the LIGO/VIRGO BH masses detected by the end of the second observing run (LVC 2018a,b). We find that the most massive BH LIGO/VIRGO has so far detected is consistent with the upper edge of the BH masses we find. This is due in part, to the large 90% confidence intervals on the individual BH masses from GW detections. Nevertheless, even when considering the much better determined chirp mass of GW170729, it remains within the maximum chirp mass predicted assuming random pairing of BHs with mass ratio $q = M_2/M_1 > 0.5$ (Marchant et al. 2018).

Figure 6.3 shows, as a function of Z, what is the final fate of the mass inside the progenitor star forming the most massive BH.

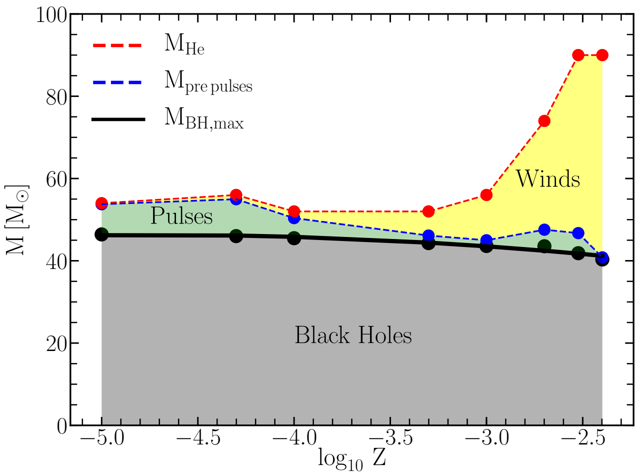

Fig. 6.3: Fate of the mass of the progenitors of the most massive BH below the PISN BH mass gap as a function of metallicity. The gray region denotes mass which becomes the BH. The green region denotes mass that is lost via pulsations. The yellow region denotes mass loss via winds. Black points denote the final BH mass. Blue points denote the edge between mass loss in pulsations and in winds. Red points mark the initial helium core mass of the star.

At low metallicities, the weakness of the stellar winds results in most of the initial stellar mass of the star forming the BH. At higher metallicites wind mass loss is able to drive approximately half of the initial mass away before the star collapse to form a BH. The stars making the most massive BHs only lose $1-5\,M_{\odot}$ of material in the pulsations.

Our models span over 2.5 orders of magnitudes in metallicity, but over such a wide range the maximum BH mass decreases only slightly between $\mathrm{M_{BH,Max}} = 40 - 46\,\mathrm{M_{\odot}}$. This corresponds to a 15% variation, for BHs whose progenitor underwent a PPISN. The initial helium core mass which forms the most massive BHs at each Z increases from $\sim 54\,M_{\odot}$ at $Z = 10^{-5}$ to $90\,M_{\odot}$ at $Z = 4\times10^{-3}$. This increase in mass is not due to changes in pulse behavior, but instead to the increased mass loss due to winds (seen as the yellow shaded region in figure 6.3). Thus with a change of only $6\,M_{\odot}$ in BH mass, the initial mass needed to produce the BH changes by $\sim 40\,M_{\odot}$ due to changing the metallicity over 2.5 orders of magnitude.

6.5 Physics dependence of the gap

In figure 6.4, we show the variations in the BH mass distribution for multiple assumptions of stellar physics, varied within either their theoretical or experimentally derived uncertainties. Each model is computed at a fixed metallicity of $Z = 10^{-3}$, with only one parameter varied in each model.

6.5.1 Wind prescription

Figure 6.4(a) shows the effect of different mass loss prescriptions on the CO-BH mass distribution. Overall the difference in masses between the different prescriptions (and η values) is small. The different prescriptions bifurcate into two groups, those where $\mathrm{M_{BH,max}} \sim 44\,\mathrm{M_{\odot}}$ (Hη = 0.1 and N&Lη = 0.1) and those with $\mathrm{M_{BH,max}} \sim 48\,\mathrm{M_{\odot}}$ ($\dot{\mathrm{M}} = 0.0$, N&Lη = 1.0, and T (with both $\eta' s$)). The models producing smaller maximum BH masses, also shift their

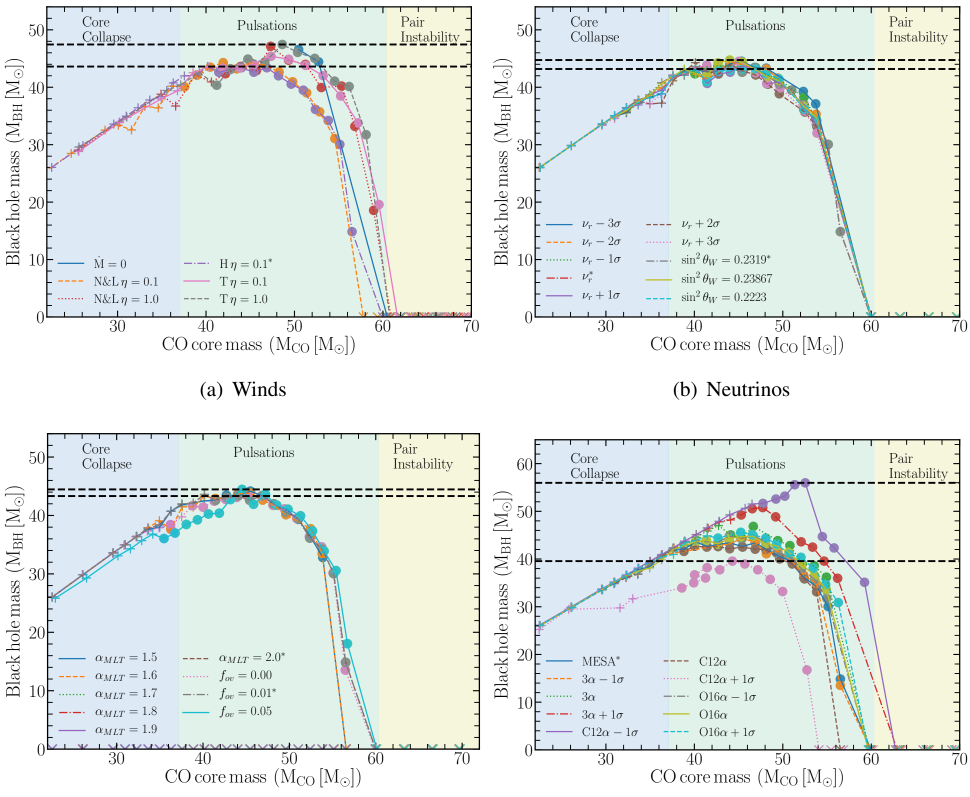

(a) Winds (b) Neutrinos

(c) Mixing (d) Nuclear reaction rates

Fig. 6.4: BH mass as function of CO core mass for different physics assumptions. Panel a shows variations in the wind mass loss prescription; H is the prescription of Hamann & Koesterke (1998), N&L is the prescription of Nugis & Lamers (2000), and T is from Tramper et al. (2016), while η varies between 0.1 and 1.0. Panel b shows variations in the neutrino physics; due to the numerical uncertainties in the fits (Itoh et al. 1996), each sigma represents a scaling of this uncertainty; and the Weinberg angle. Panel c shows variations in the convective treatment, with varying MLT scale heights α_{MLT} and convective overshoot values $f_{\rm ov}$. Panel d shows variations in a select set of nuclear reaction reactions; `MESA`'s default rates are from `NACRE` (Angulo et al. 1999a) and `REACLIB` (Cyburt et al. 2010), while the other rates come from `STARLIB` (Sallaska et al. 2013) as either the median or $\pm 1\sigma$ uncertainties, 3α is the triple alpha reaction, C12α is the ^{12}C$\,(\alpha,\gamma)^{16}\,$O reaction, and O12α is the ^{16}O$\,(\alpha,\gamma)^{20}\,$Ne reaction. Plot symbols have the same meaning as in Figure 6.2. A star represents our default model assumptions for each physics variation. Dashed lines indicate the range of locations for the edge of the BH mass gap. Colour shading shows the regions between the CC, PPISN, and PISN outcomes for our fiducial set of physics assumptions.

transition to PISN to smaller CO core masses. These models lose more mass via winds and come from $M_{\rm He}int \sim 64\,M_\odot$. The second group, which make $M_{\rm BH,max} \sim 48\,M_\odot$, come from $M_{\rm He}int \sim 58\,M_\odot$ cores and lose less mass via winds. As the strength of mass loss increases, either though changing the wind prescription or increasing the metallicity, the CO-BH mass distribution flattens and decreases the maximum BH mass. There is no set of models (H) with

$\eta = 1.0$ shown, as the amount of mass loss when using this prescription is sufficient that no model enters the pulsation region.

6.5.2 Neutrino Physics

Figure 6.4(b) shows the BH mass as a function of the CO core mass for variations in the neutrino rate and the Weinberg angle. Between $\pm 3\sigma$ in the neutrino rates the overall effect is small. As we vary the rates from their -3σ value to their $+3\sigma$ we find little change in the BH mass distribution, with the maximum BH mass varying by $\sim 1\,M_\odot$ and a trend for less massive BHs as the neutrino rate increases. As the Weinberg angle varies, again the CO-BH mass function is approximately constant. Smaller Weinberg angles result in a slightly lower maximum BH mass, with a variation of $\sim 1.5\,M_\odot$ for the range of $\sin^2\theta_W$ considered here.

6.5.3 Convective mixing

Figure 6.4(c) shows variations in $\alpha_{\rm mlt}$ between 1.5 and 2.0, with our default assumption being $\alpha_{\rm mlt} = 2.0$. Within these limits there is very little change in the behavior of the BH masses, with the BH masses slightly decreasing as $\alpha_{\rm mlt}$ increases.

Figure 6.4(c) also shows the effect of varying $f_{\rm ov}$ to be small. The maximum BH mass varies within $1\,M_\odot$ over the range considered here. The most significant difference occurs at the PPISN/CC boundary where $f_{\rm ov} = 0.05$, decreases the final BH mass relative to the lower $f_{\rm ov}$ models. This is due to a change in behavior in the burning and convection regions at the center of the star. When $f_{\rm ov}$ is small the star has a separate off-center and a central burning region, both of which drive convection zones. When $f_{\rm ov}$ increases these convection zones can merge, which increases the available fuel supply and causes the pulses to become stronger, driving increased mass loss.

6.5.4 Nuclear reaction rates

Figure 6.4(d) shows the CO-BH mass function for different rates computed from STARLIB and our default rates from NACRE and REACLIB. Overall the effect of the $^{16}{\rm O}\,(\alpha,\gamma)^{20}\,{\rm Ne}$ is minimal on both the BH mass distribution and the maximum BH mass. However both the 3α rate and the $^{12}{\rm C}(\alpha,\gamma)^{16}{\rm O}$ rates have a large impact on both the BH mass distribution and the maximum BH mass formed.

As the $^{12}{\rm C}(\alpha,\gamma)^{16}{\rm O}$ rate decreases the maximum BH mass increases, for $+1\sigma$ we find $M_{\rm BH,max} = 40\,M_\odot$ while at -1σ we find $M_{\rm BH,max} = 58\,M_\odot$. Thus within the 68% confidence interval for the C12α the maximum BH mass varies by $\sim 18\,M_\odot$ [3] . The median $^{12}{\rm C}(\alpha,\gamma)^{16}{\rm O}$ rate from STARLIB, from Kunz et al. (2002), is smaller than the NACRE rate, thus STARLIB predicts a more massive maximum BH mass. deBoer et al. (2017) also provide an updated

[3] For $^{12}{\rm C}(\alpha,\gamma)^{16}{\rm O}$ reactions with the $+1\sigma$ rate, we burn sufficient ^{12}C during core helium burning such that we never trigger the CO core mass definition in section 6.2. Thus we relax our CO core mass definition to be the mass coordinate at the maximum extent of the core helium burning convection zone.

$^{12}C(\alpha,\gamma)^{16}O$ rate which is smaller, over the core helium burning temperature range, than NACRE. Models with this rate showed a similar increase in the maximum BH mass.

As the 3α rate, from Angulo et al. (1999b), increases the maximum BH mass also increases. This correlates with the $^{12}C(\alpha,\gamma)^{16}O$ rate behavior; as 3α rate increases or the $^{12}C(\alpha,\gamma)^{16}O$ rate decreases we increase the mass fraction of ^{12}C in the core. For the values tested here, this increases from $\sim 10\%$ to $\sim 30\%$.

We find that as the mass fraction of carbon increases in the core the maximum BH mass also increases, and also alters the behavior of the pulses. Higher carbon fractions decrease the range in CO core mass within which models undergo pulsations. This would translate into a smaller predicted rate of PPISN in the Universe, as there is a smaller range of possible progenitors. Increasing the mass fraction of carbon also decreases the fraction of models with strong pulsational mass loss, by weakening the pulses such that they do not eject mass. As the carbon fraction increases the BH mass distribution sharpens (similar to what is seen with no mass loss in Figure 6.4(a)). This also shifts the boundary between CC/PPISN and between PPISN/PISN to higher masses as the carbon fraction increases. Moving the boundary between PPISN/PISN to higher CO core masses would translate to needing a more massives initial star, and thus this would decrease the predicted rate of PPISN and PISN.

We performed additional tests varying the $^{12}C+^{12}C$ and $^{16}O+^{16}O$ reaction rates[4] between 0.1 and 10 times their default MESA values as STARLIB does not have temperature dependent uncertainties for them. These rates showed variations in the maximum BH mass of $\sim 4\,M_{\odot}$, with the $^{12}C+^{12}C$ having a larger effect on the maximum BH mass.

Due to the sensitivity of the maximum BH mass to the $^{12}C(\alpha,\gamma)^{16}O$ rate, the measured value of the maximum BH mass (below the PISN mass gap) can be used to place constraints on the $^{12}C(\alpha,\gamma)^{16}O$ rate (Farmer et al, in prep).

6.5.5 Model resolution

MESA has a number of ways to control the spatial and temporal resolution of a model. Here we vary MESA's `mesh_delta_coeff`, which controls the maximum allowed change in stellar properties between adjacent mesh points during the hydrostatic evolution, between 0.8 and 0.3. Decreasing the value increases the resolution. This range corresponds to roughly a factor of two increase in the number of grid points. We also vary MESA's adaptive mesh refinement parameters (AMR), which set the resolution during hydrodynamical evolution. We vary `split_merge_amr_nz_baseline` between 6000 and 10000 and `split_merge_amr_nz_MaxLong` between 1.25 and 1.15, where the second values denotes a higher resolution. This leads to and increase by a factor of two in the number of spatial zones during the evolution of a pulse.

We have also varied MESA's `varcontrol_target`, which sets the allowed changed in stellar properties between timesteps, between 5×10^{-4} and 5×10^{-5}, and varied the `max_`

[4]In the `approx21.net` nuclear network these reactions rates are compound rates where the different output channels have been combined.

`timestep_factor` between 1.025 and 1.05, which sets the maximum timestep factor by which `MESA` can increase a timestep. This leads to an increase of $\sim 30\%$ in number of timesteps taken. Over the ranges considered here we find changes of $\sim 1\,M_{\odot}$ in the maximum BH mass.

Over the range of nuclear networks considered here; `approx21.net`, `mesa_75.net`, `mesa_128.net`; there is little change in the BH mass for a given CO mass, by at most $\sim 1\,M_{\odot}$. There is a trend for larger nuclear networks to produce slightly more massive BHs.

Woosley (2017) suggest that PPI systems need large nuclear networks which can adequately follow weak interactions, which `approx21.net` does not follow. However both the CO-BH mass relationship, and the maximum BH mass vary within $\sim 1\,M_{\odot}$ over the networks considered here. Changing the isotopes evolved will have an effect on the composition and final structure of the star as well as the composition of the ejecta from the pulses. However, we find that much of the behavior that determines the final BH mass is set by the conditions at the initial pulse. This is set by the CO core mass and carbon mass fraction, both of which are set by core helium burning, which is not affected by the lack of weak reactions in `approx21.net`.

6.6 The maximum black hole mass and its implications

Figure 6.5 summarizes the range in the maximum BH mass below the PISN gap due to the variations considered in sections 6.4 and 6.5. These include those affected by the environment (metallicity) and thus vary across the Universe, those for which we have incomplete or uncertain physics (Rates, winds, $\alpha_{\rm mlt}$, $f_{\rm ov}$, $\nu_{\rm rate}$, and $\sin^2\theta_W$) but we expect to be constant in the Universe, and those that are model dependent (spatial, temporal, and nuclear network resolution). For most of the physics for which we are uncertain ($\alpha_{\rm mlt}$, $f_{\rm ov}$, $\nu_{\rm rate}$, and $\sin^2\theta_W$) and the model resolution (spatial, temporal, and in number of isotopes) there is a limited effected on the maximum BH mass. These terms place $\sim 2\,M_{\odot}$ uncertainties on the maximum BH mass, over the ranges considered here, contingent on how the different uncertainties are combined.

The next most significant factors are the metallicity and winds. We consider these together, since the metallicity dependence of wind mass loss rates introduces a degeneracy between these two elements. As we observe a population of BHs from different progenitor stars with varying metallicities, then this 15% variation in the maximum BH mass places a minimum level of uncertainty on what we can learn from the most massive BHs detected. Given a sufficiently large population of binary BHs (at multiple redshifts) it may be possible to disentangle the effects of the star formation and metallicity evolution of the Universe on the BH population (Dominik et al. 2013; Dvorkin et al. 2016). However this uncertainty which varies over the Universe, is small compared to the current measurement uncertainties. This could allow the maximum BH mass to be used as a standard siren, as the maximum BH mass varies slowly with the chemical evolution of the Universe.

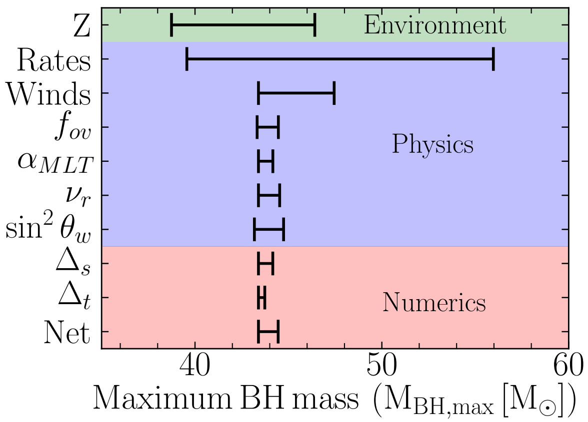

Fig. 6.5: Range of maximum BH masses, for different environment and stellar physics assumptions. See Figure 6.2 for the range of metallicities considered here, see Figure 6.4 for the ranges of each physics assumption.

The most significant physics variation considered here is due to the nuclear physics uncertainties, and primarily due to the $^{12}\mathrm{C}(\alpha,\gamma)^{16}\mathrm{O}$ rate, leading to a 40% variation in the maximum BH mass. Models having lower $^{12}\mathrm{C}(\alpha,\gamma)^{16}\mathrm{O}$ rates lose less mass in pulsations and thus produce more massive BHs. Thus, even with a lack of knowledge about the environment in which any individual BH formed, we can still use the detection of sufficiently massive BHs to constrain nuclear physics. The most massive detected BH indicates the maximum value for the $^{12}\mathrm{C}(\alpha,\gamma)^{16}\mathrm{O}$ rate over the core helium burning temperature range.

Given the sensitivity of the BH mass to the CO core mass, the maximum BH mass formed is effectively independent of its stellar origin. Assuming that both chemically homogeneous evolution or common envelope evolution can produce a sufficiently massive, H-poor, He core we would expect those evolutionary scenarios to merging BHs to result in similar final BH masses.

6.7 Comparisons to other work

In Yoshida et al. (2016) they studied PPISN from stars with initial masses between 140 and 250 $M_\odot$ and Z=0.004. They find the final masses of their stars to be between 50 and 53 $M_\odot$ at collapse, broadly consistent with the masses we find. For our models at Z=0.004 we would expect slightly smaller BHs, due to the winds stripping the outer CO layers of the stars. Another possible source of differences may be the choice of the Caughlan & Fowler (1988) $^{12}\mathrm{C}(\alpha,\gamma)^{16}\mathrm{O}$ rate (Yoshida & Umeda 2011).

Our models agree with the wind-less, metal-free, helium-core models of Woosley (2017), who finds a maximum final BH mass 48 $M_\odot$. This agrees with our wind-less, models where we also find a maximum BH mass of 48 $M_\odot$ (though we evolve them at a non-zero metallicity). Woosley (2017) also find a maximum BH mass of 52 $M_\odot$ for models which did not remove their entire hydrogen envelope. Although they are not directly comparable to our results, which assume all helium has been removed, they provide bounds on the variation in the maximum BH mass, if the H-envelope is not completely removed, of $\sim 4\,M_\odot$. Woosley (2019) investigated the evolution of naked He cores finding a maximum BH mass below the gap of 46 $M_\odot$ in agreement with our results, for our default $^{12}C(\alpha,\gamma)^{16}O$ rate and assumptions on metallicity.

Takahashi (2018) looked at the effect of varying the $^{12}C(\alpha,\gamma)^{16}O$ rate on the boundary between PPISN and PISN. Our results are not directly comparable as they used the Caughlan & Fowler (1988) rate, while by default we use the `NACRE` rate. They found that as the $^{12}C(\alpha,\gamma)^{16}O$ rate decreases, which increases the ^{12}C fraction, the PISN boundary shifts to higher initial masses, similar to our findings. Takahashi (2018) also find a narrowing of the PPISN region (in initial mass space), consistent with our results.

Leung et al. (2019) studied the evolution of helium cores between $80 - 140\,M_\odot$ and $Z = 10^{-3} - 1.0Z_\odot$, with a previous `MESA` release (version 8118) and a different treatment of the hydrodynamics. Their results are in agreement with ours. They find a maximum BH mass of $\sim 50\,M_\odot$, which is larger than what we predict, likely due to their lowest metallicity models ($Z = 10^{-2}Z_\odot$) having no wind mass loss. Our no mass-loss models at $Z = 10^{-3}$ have a maximum BH mass of 48 $M_\odot$. At higher metallicities we find that wind mass loss is sufficient to make the maximum BH come from a CC event rather than a PPISN. The remaining differences may be due to other differences in choice of parameters and/or changes between the two `MESA` versions.

In this work we did not consider the effects of rotation on the stellar progenitors, which is especially important if they came from chemically homogeneous evolution (de Mink et al. 2009; de Mink & Mandel 2016b; Marchant et al. 2016). However, Chatzopoulos & Wheeler (2012a,b) have previously studied the impact of rotation on zero metallicity models evolved first with `MESA` and then `FLASH`, in 1-D, for the dynamical evolution. They found that increasing the rotation rate the initial mass for PPISN or PISN decreases. This is due to the increase in CO core mass due to rotational mixing. They find PPISN from stars with core masses between $\sim 40 - 65\,M_\odot$, which agrees with our results. However the impact of centrifugal support on the resulting BH masses from PPISN is an open problem.

6.8 Summary and conclusions

The prediction of a gap in the mass distribution of BHs from the collapse of stars dates back to the sixties, when the theory of pair instability evolution had first been developed (Fowler & Hoyle 1964; Barkat et al. 1967). However, it is only recently that the possibility of testing this prediction directly with gravitational waves has opened. As the presently observed population of binary BHs is compatible with having stellar origin (LVC 2018a,b), instead of dynamical or primordial, we can use stellar evolution models to interpret the upper end of the BH mass distribution.

We find that the evolution of single bare He cores robustly predicts a maximum BH mass of $\sim 45\,M_\odot$, and that this value is relativity insensitive to variations in the input physics, the algorithmic approach, and the metallicity of the models. In particular, despite the uncertain wind mass loss rates of massive stars, we find a variation of the maximum BH mass of only

$\sim 15\%$ (from $\sim 40\,M_{\odot}$ to $\sim 46\,M_{\odot}$) over 2.5 orders of magnitude in metallicity. This implies that detailed knowledge of the host galaxy of merging binary BHs is not required to use gravitational wave detections to probe the physics of the unobserved stellar progenitors.

The insensitivity to metallicity of the maximum BH mass below the gap might also allow for cosmological applications. If its value can accurately be determined, it might provide a "standard siren" (e.g., Schutz 1986) to break the degeneracy between luminosity distance and total mass of observed merging BH binaries.

Assuming a stellar origin, the most massive BHs detected below the pair instability mass gap might be used to further constrain nuclear physics, specifically the $^{12}C(\alpha,\gamma)^{16}O$ reaction in the core helium burning regime. In particular, the maximum BH mass puts an upper limit on this reaction rate. Other physics variations including neutrino physics, wind algorithms, and chemical mixing have sub-dominant effects on the maximum BH hole mass and negligible contributions to the uncertainty compared to the typical observational uncertainties.

We note however that our estimates of the BH mass may be over-predicted if, for instance, a significant amount of mass is loss via neutrinos during the final collapse (Coughlin et al. 2018). Also, our simulations do not account self-consistently for binary interactions between the progenitor stars, which deserves further attention (Marchant et al. 2018).

If BHs with masses inside the predicted PISN mass gap are detected they should either have non-stellar origin or be the result of multiple mergers in a cluster (Rodriguez et al. 2016b; Stone et al. 2017). However, Gerosa & Berti (2019) claim that only systems where both BHs have already previously merged can appreciably populate the predicted gap, with the rate of forming a binary BH dropping with each merger event, due to recoil from a merger ejecting the BH from the cluster. Whether BHs are ejected from clusters also depends strongly on whether they are born spinning; if they do not spin then they are more likely to stay bound in the cluster (Rodriguez et al. 2019).

The present and upcoming detections of binary BH mergers might provide evidence constraining the death of the most massive stars before we might be able to unequivocally observe these phenomena in the electromagnetic spectrum (Stevenson et al. 2019). Our results suggest, that with a large population of merger events, we can put constraints on uncertain nuclear physics and provide a new tool for cosmology.

We acknowledge helpful discussions with B. Paxton, F. Timmes, and I. Mandel, Y. Götberg, D. Hendriks, E. C. Laplace, E. Zapartas. RF is supported by the Netherlands Organization for Scientific Research (NWO) through a top module 2 grant with project number 614.001.501 (PI de Mink). SdM and MR acknowledge funding by the European Union's Horizon 2020 research and innovation programme from the European Research Council (ERC) (Grant agreement No. 715063), and by the Netherlands Organization for Scientific Research (NWO) as part of the Vidi research program BinWaves with project number 639.042.728. PM acknowledges support from NSF grant AST-1517753 and the Senior Fellow of the Canadian Institute for Advanced Research (CIFAR) program in Gravity and Extreme Universe, both granted to Vassiliki Kalogera at Northwestern University. This work was carried out on the Dutch national e-infrastructure with the support of SURF Cooperative. This research has made use of NASA's Astrophysics Data System.